Journal of Hydroscience and Hydraulic Engineering
Vol. 29, No.1 May, 2011, 123-135

DEVELOPMENT OF SPACE TIME IMAGE VELOCIMETRY INTRODUCED FAST FOURIER TRANSFORM FOR IMPROVING ROBUSTNESS IN RIVER SURFACE FLOW MEASUREMENT

By

Ichiro Fujita

Department of Civil Engineering, Graduate School of Engineering, Kobe University, Nada, Kobe, Japan

and

Hiroki Hara

Graduate Student, Department of Civil Engineering, Graduate School of Engineering, Kobe University, Nada, Kobe, Japan

SYNOPSIS

As one of the non-contact river flow measurement methods, an image analysis method using space-time image of river surface flow, namely space-time image velocimetry (STIV), has been developed by the authors. In this method, a space-time image (STI) for a line segment placed along the streamwise direction can be generated, whereby which streamwise surface velocity can be extracted from the mean gradient of a striped pattern that appeared in the STI. Originally, STIV applies an image smoothing filter to an STI for improving the measurement accuracy in order to remove non-negligible noise in the STI. However, this still poses difficulty in measuring deteriorated space-time images obtained during adverse weather conditions. In the method presented in this work, we transformed the STI into a frequency domain by using a 2D fast Fourier transformation (FFT) to extract only the information directly related to surface flow. The treatment of STI improves the measurement accuracy and also allows us to analyze wave length and celerity distribution of surface waves generated during floods.

INTRODUCTION

River flow velocity distribution and river discharge are one of the most important and also the most difficult-to-measure hydrological parameters in river engineering. The conventional method for discharge measurement used mainly in Japan and Korea is to use several floats to measure mean velocities along their paths and to integrate them over the cross-sectional area. Although the float method is robust and applicable to various conditions, it becomes quite difficult to adopt this method in large flood conditions because manual operations near the river or from a bridge sometimes become extremely dangerous to continue. Moreover, the traceability of floats to the flow becomes questionable in a significant turbulent condition accompanying vortical flow. Therefore, alternative methods such as acoustic Doppler current profiler (ADCP) (Muste et al. (11), Dinehart and Burau (1), Oberg and Mueller (13)), side-looking ADCP (Le Coz et al. (9)), UHF radar (Teague et al. (14), Wang et al. (15)) or imaging

techniques have been developed in the last decade. While the first two methods measure three-dimensional velocity distributions within the water, the latter methods measure one- or two-dimensional surface velocity distributions by assuming that water surface roughness is convected with the surface flow in flood flow conditions.

Among the above methods, imaging techniques such as the large-scale particle image velocimetry (LSPIV) (Fujita and Komura (2), Fujita et al. (3), Fujita, et al. (4), Kantoush et al. (8), Meselhe et al. (10), Jedeau et al. (7), Hauet et al. (6), Muste et al. (12)) and the space-time image velocimetry (STIV) (Fujita et al. (5)) are good options for establishing economical flow measurement system, because even a personal camcorder can be employed for obtaining raw information for the analysis. In contrast to LSPIV, STIV is robust under various conditions which cause the deterioration of water-surface image quality. The image-quality deterioration occurs in cases where raindrops adhere to the filter in a severe rain and wind conditions, or in cases where the images contain frame-dropping in the nighttime recording with insufficient surrounding light. In fact, it is difficult for LSPIV to provide reasonable data in the above-mentioned conditions. In the present research, a new image filtering method using a two dimensional fast Fourier transformation (2D-FFT) is introduced to improve the accuracy and efficiency of STIV under severe conditions for LSPIV. Moreover, the characteristics of surface wave celerity and wave length are investigated from the spectral analysis of decomposed images from an STI.

OUTLINE OF THE ORIGINAL STIV

The outline of the original STIV developed by Fujita et al.(5) is shown in Fig.1 through its application to the flood flow measurements taken in the Chikusa River on July 14, 2007. Firstly, we set a line segment parallel to the main flow direction as shown in Fig. 1(a). The direction of the line segment can be determined either by an LSPIV manner or by a visual inspection assuming that flood water flows parallel to the river bank. Although the physical length of the line segment required for the analysis varies with the scale of the river, its length does not usually exceed the river width; therefore the line segments can be aligned parallel to the river bank even at a river bend from a practical point of view. Secondly, an STI is generated by taking brightness distribution in the line segment as the horizontal axis and its evolution with time as the vertical axis (Fig. 1(b)). It is evident that an inclined pattern is generated in the STI displaying convection of surface ripples with the surface flow. The mean gradient of the pattern corresponds to the local mean velocity along the line segment. It should be noted that the mapping relation between the physical coordinates and the screen coordinates has to be predetermined as in the case of LSPIV in order to calculate the actual physical length of the line segment. Thirdly, the orientation angle ? for each of a small segment on STI is calculated in accordance with the following relation (Fujita et al. (5)):

$$tan\,2\phi = \frac{2J_{xt}}{J_{tt} - J_{xx}} \tag{1}$$

where

$$J_{xx} = \int_A \frac{\partial g}{\partial x}\frac{\partial g}{\partial x} dxdx \tag{2}$$

$$J_{xt} = \int_A \frac{\partial g}{\partial x}\frac{\partial g}{\partial t} dxdt \tag{3}$$

$$J_{tt} = \int_A \frac{\partial g}{\partial t}\frac{\partial g}{\partial t} dtdt \tag{4}$$

$g(x,t)$: grey level intensity on STI and A is the area of the small segment. Fig.1(d) presents the distribution of the coherency defined by

$$C = \frac{\sqrt{(J_{tt} - J_{xx})^2 + 4J^2_{xt}}}{J_{xx} + J_{tt}}, \tag{5}$$

which is a measure of the image pattern coherence and takes a value between zero and one; for an ideal local orientation its value becomes one and for an isotropic gray image it becomes zero. Therefore, it is possible to calculate the mean orientation angle by preferably obtaining clearer orientation information taking coherency as a weighting function:

$$\bar{\phi} = \int \phi C(\phi) d\phi / \int C(\phi) d\phi \,. \tag{6}$$

Fig.1(e) is a weighted histogram of the orientation angle, showing distribution with a sharp peak. Finally, since the length and time scales of the STI are given, the mean velocity along the line segment can be calculated.

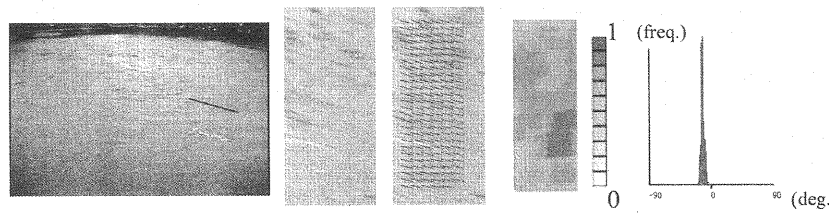

Fig. 1 Outline of STIV procedure for the Chikusa River flood, 19:10 July 14, 2007: (a) set line segment, (b) generate STI (horizontal size=4.65m, vertical size=10s), (c) calculate orientation angles (d) calculate coherency (e) generate histogram of orientation angles

IMAGE RECORDING SYSTEM

In the present river observation system, we utilized a monitoring video camera, CCTV, already installed by the local government on the right bank of the Chikusa River as shown in Fig.2. However, since it was difficult to send movie data to the local office in real time with the existing slow transmission system, we setup an onsite timer-controlled recording system with a 1TB hard disk (HD), in which the analogue data from the CCTV is directly transferred to the hard disk. The timer was set up so that the movie was repeatedly recorded for one minute after waiting for nine minutes. With the prepared HD, almost fifty days of movie data can be stored in the present system. Therefore, the image analysis had to be conducted after the flood occurred in the present system.

The hydrograph of the target flood at the site is provided in Fig.3 together with representative surface images at several time zones ranging from daytime to nighttime. In this flood, the peak water level of about 3.71m occurred around 7:30pm on July 14. At this stage, the water level exceeded the flood plain level slightly. Hence, the water surface width extended more than that of the lower channel up to the maximum width of about 81m. As indicated in Fig.3, the image quality is not always favorable for the image analysis in this flood, because in some cases images are obstructed by raindrop adherence to the lens filter and in the other cases, frame dropping occurs due to insufficient illumination by surrounding street light sources. Such image deterioration makes it difficult to apply LSPIV directly to these images. These difficulties in flow measurements can be overcome by the application of the new STIV techniques

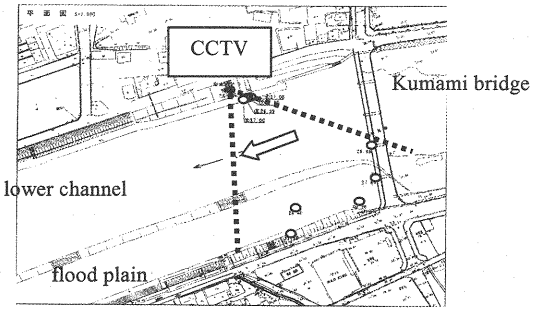

Fig. 2 CCTV location at the Chigusa River; filled black circle: CCTV location, white circles: mark points for mapping screen and physical coordinates

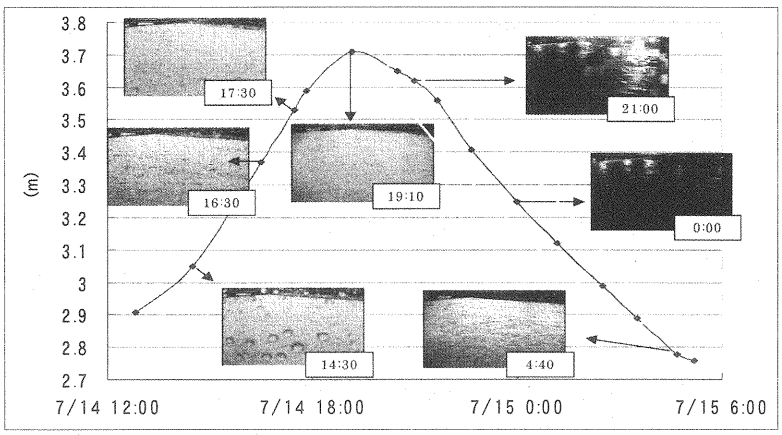

Fig. 3 Water level hydrograph and surface images in 2007 Flood

which will be explained in the following sections.

APPLICATION OF 2D-FFT FILTERING

Two examples of STI with image deterioration caused by raindrop adherence and frame-dropping are respectively shown in Fig.4(a) and Fig. 4(b). Here the horizontal axis corresponds to the line segment and the vertical length indicates time axis. The effect of raindrop appears as a vertical dark thick line, while the frame-dropping effect is seen as a step-like pattern. In the first place, direct application of the original STIV to these STI yields false orientation vectors as shown in Fig.5. The orientation vectors are generated along the thick vertical line caused by the raindrop effect in Fig.5(a) and follow horizontal and vertical step-like patterns in Fig.5(b). Therefore, the histogram of the orientation angle for each case in Fig.6 tends to demonstrate distribution with no significant peak.

In order to correct the erroneous orientation vectors, we applied a 2D-FFT to an STI for noise reduction through band pass filtering. As an example, transformed images of Fig.4 are provided in Fig.7. The unit of the axes is the wave number. It is clear that a pattern corresponding to the stripes in the original STI appears vaguely in the transformed images. Fig.8 simply illustrates the method to apply high-pass or low-pass filtering. Since the wave components of low frequencies are distributed in the center of the FFT image, high-pass filtering can be performed by deleting the information in the central region of the FFT image as shown in Fig.8(a). On the other hand, a low-pass filtering can be

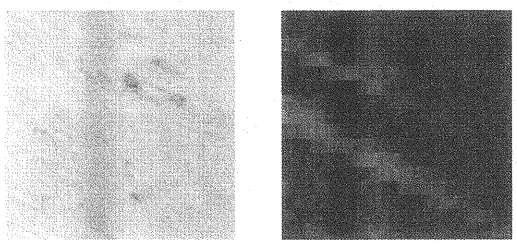

(a) (b)

Fig. 4 Deteriorated STI images: (a) raindrop adherence, (b) frame. dropping; horizontal length indicates line segment, vertical axis time scale

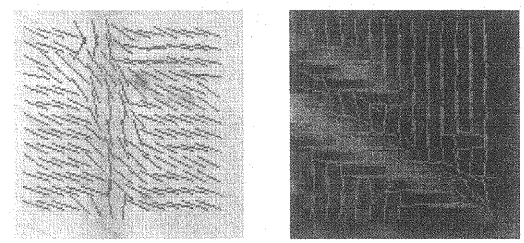

(a) (b)

Fig. 5 Orientation vectors by direct application of STIV; note the caption of Fig.4 for (a) and (b)

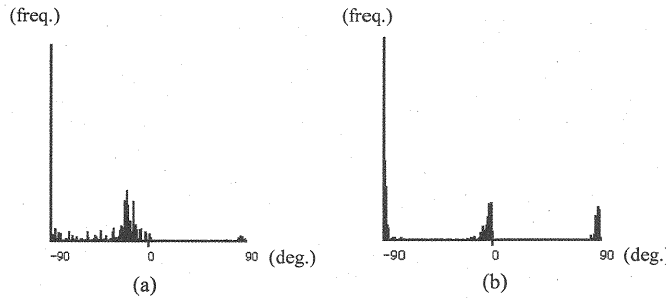

Fig.6. Histogram of orientation angles by direct application of STIV; note the caption of Fig.4 for (a) and (b)

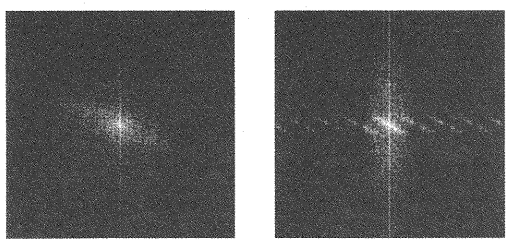

(a) (b)

Fig. 7 Fourier transformed images; note the caption of Fig.4 for (a) and (b)

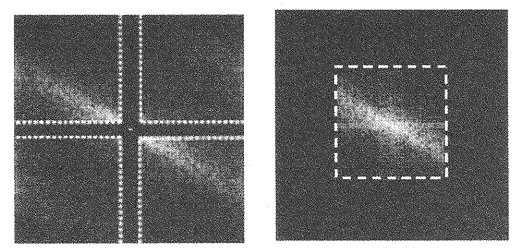

(a) High-pass filter (b) Low-pass filter

Fig.8 High pass and low pass filtering on FFT image

conducted by keeping the information only in the central region of FFT image as illustrated in Fig.8(b). By combining high- and low- pass filtering, we can apply band-pass filtering to FFT images. In fact, the quality of STI significantly improves by applying the band-pass filtering to its FFT image and subsequently by applying the inverse Fourier transformation to the filtered FFT image to recover the physical domain. Although this method is rather a popular technique in the field of image analysis, it has never been applied to space-time images of river flows.

The quality-improved STIs by such a procedure shown in Fig.9 indicate that the trace of a raindrop as well as a step-like pattern has almost disappeared from the original STIs. STIV results applied to these STIs are shown in Fig.10, with successful generation of favorable orientation vectors. Such improvements in the image quality can also be verified in the histogram of orientation angles shown in Fig.11. It is evident that a sharp peak appears in each

distribution providing evidence of improvement of measurement accuracy by the proposed procedure. It is worth mentioning again that the LSPIV is incapable of applying to these deteriorated image conditions sometimes encountered in flow measurements during floods.

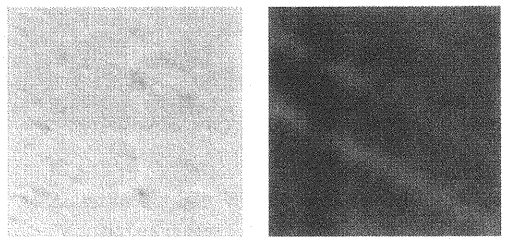

(a) (b)

Fig.9 STIs with quality improvement by band pass filter using FFT; note the caption of Fig.4 for (a) and (b)

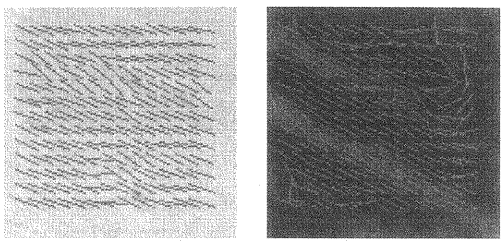

(a) (b)

Fig. 10 Orientation vectors applied to band-pass filtered STI; note the caption of Fig.4 for (a) and (b)

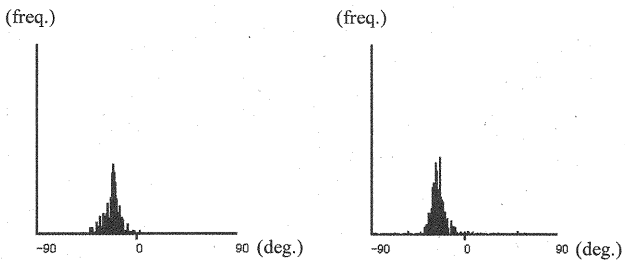

Fig.11 Histogram of orientation angles after FFT filtering; note the caption of Fig.4 for (a) and (b)

Another optional method is to apply STIV directly to the FFT image. As can be seen from Fig.12, the general orientation angle of the pattern which appears in the wave number domain is almost equivalent to that in the original STI. Therefore, the application of STIV to the FFT image with a template size comparable to the image size itself is enough to obtain the orientation angle as indicated in Fig.12(b). The broken lines indicate the calculated orientation angle. No histogram analysis is required in this method. The problem with such a method is that FFT image is subject to noise effects when the target STI includes an inconsistent pattern induced by various waves with different speeds.

MEASUREMENT OF VELOCITY EVOLUTION

To compare the performance of the several methods presented previously, the evolution of streamwise velocity components are compared for a line segment No.10 indicated as a thick line in Fig.13. The flow direction is from left to right in the figure. As a result of various image analysis techniques of the surface flow, Fig.14 shows the time variation of surface velocity during the flood. Here, STIV stands for the original STIV which applies an image smoothing filtering to a raw STI; manual STIV measures the orientation angle by means of a mouse operation with visual inspection after generating an STI, HL-STIV using the band pass filtering in the Fourier domain; FP-STIV applies STIV directly to the FFT image and LSPIV is the conventional pattern matching technique. Obviously, LSPIV yields underestimated velocity most of the time. The cause of this discrepancy can be attributed to the effects the image deteriorations, in which the general movement of image pattern are fixed or restricted at raindrop position or

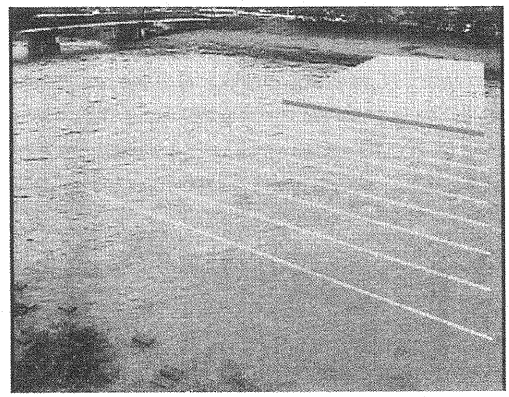

Fig.13 Location of the line segment No.10

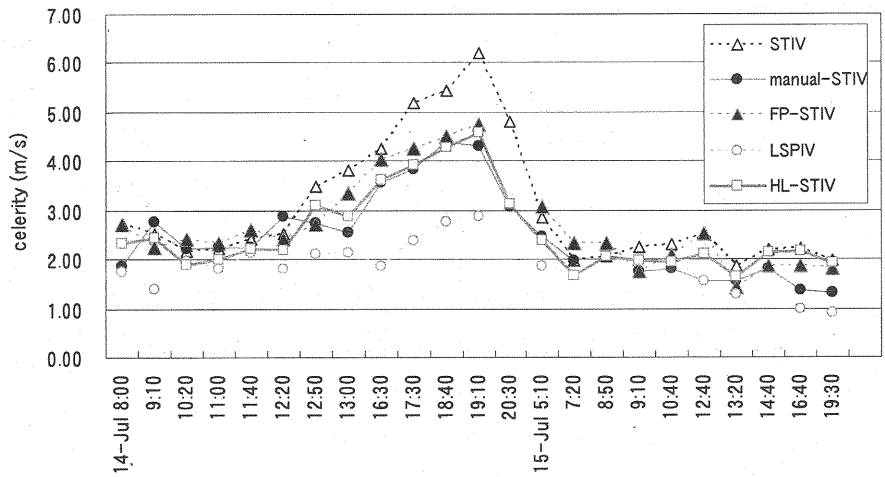

Fig.14. Measurements of streamwise velocity by various methods

step-like pattern, yielding smaller values than the actual velocity. Among STIVs, the original STIV seems to yield overestimated values in the night measurements. The reason for this difference is that the insufficient performance of the image smoothing filter applied to the raw STI under the effects of raindrop or frame dropping. For example, the effect of raindrops like the vertical trace in Fig.4(a) cannot be removed just by applying a smoothing filter to a raw STI. On a separate note in the present discussion, we treat the manual STIV as a reference because visual inspection by the human eye seems to be the proper way of finding the mean orientation angle even when the STI contains significant noise. However, of course, it is infeasible to use the manual STIV in establishing a real time analysis system because of the time consumption. Therefore, we conclude that the ideal method should generate velocity data comparable to that by the manual STIV. Comparing results by various versions of STIV indicated in Fig.14, HL-STIV yields almost equivalent results to the manual STIV with the least relative difference. It should be noted that the data is obtained without any manual operation in HL-STIV. FP-STIV also yields favorable results but with a greater variation when the STI contains noisy patterns.

As has been demonstrated so far, each STI includes inclined striped patterns representing the celerity of water surface ripples with various wave lengths. To examine the characteristics of surface waves on flood flow, we applied spectral analysis to an STI. The STI and its 2D-FFT image which were examined are shown in Fig.15. In the present case, the horizontal length of STI is 14.0m and its vertical length is 8.53 seconds. The image size, 256 by 256 pixels, is

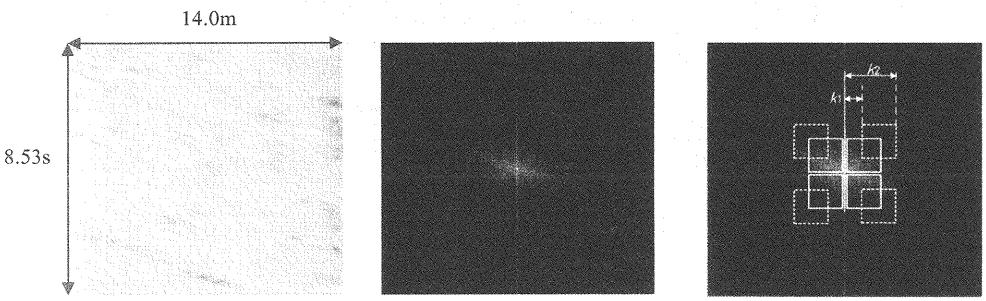

(a)Original STI (b) Spectral image

Fig.15 STI and its FFT image

Fig.16 Filtering range on spectral image

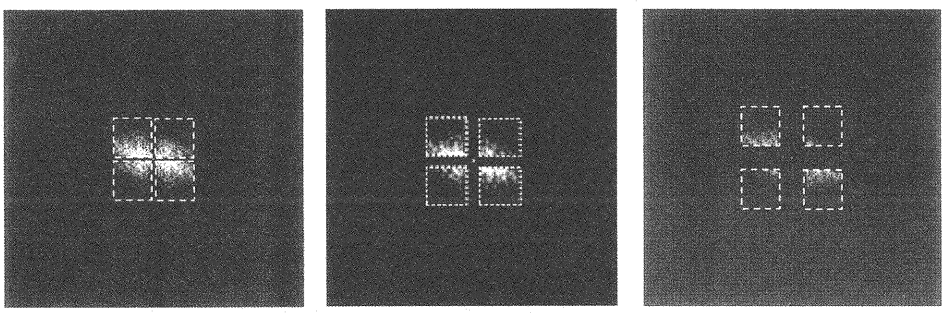

(a) CASE 1 (b) CASE 4 (c) CASE 10

Fig.17 Spectral image after selecting frequency range

the same before and after applying 2D-FFT. Since one pixel indicates one wave length in the FFT image, we can count the wave number only in integer unit, i.e. the number of waves that can be produced within the horizontal length of 14.0m. In the present approach, we begin by setting a range of band pass wave number between lower and higher values, as k1 and k2 , respectively, and by keeping their difference constant, which is illustrated in Fig.16 Subsequently, an STI image including only the selected range of wave numbers is reproduced by applying the inverse FFT to the filtered FFT image as shown in Fig.17. For example, CASE 1 picks up pattern with shorter waves, while CASE 10 contains waves with longer wave length and CASE 4 picks up the intermediate waves. Finally, STIV is applied to the band-pass-filtered STI image and the wave celerity of surface ripples is calculated.

The examined range of band-pass filter and the related minimum and maximum wave lengths are shown in Table 1. The lower wave number k1 is varied from one and ten. The value of k1 corresponds to the maximum wave length varied here between 1.4m and 14m. It should be noted that observable maximum wave length is the same as the length of the line segment or horizontal length of STI. On the other hand, the value of k2 indicates the minimum wave length, which is varies between 0.33m and 0.42m in the present case. This implies that minimum wave length is kept almost

constant in the present examination. Therefore, the present analysis virtually examines the effect of the maximum wave number to the celerity of surface ripples. To demonstrate the effect of filtering, three examples of filtered STI are shown in Fig.18 for CASE 1, CASE 4 and CASE 10. It is clear that the pattern in STI for CASE 1 which contains most of the wave components is significantly different from CASE 10 containing shortest wave components and CASE 4

Table 1 Range of band-pass filter and wave length

CASE	k_1	k_2	λ min(m)	λ (max)
1	1	33	0.424	13.978
2	2	34	0.411	6.989
3	3	35	0.399	4.659
4	4	36	0.388	3.494
5	5	37	0.378	2.796
6	6	38	0.368	2.33
7	7	39	0.358	1.997
8	8	40	0.349	1.747
9	9	41	0.341	1.553
10	10	42	0.333	1.398

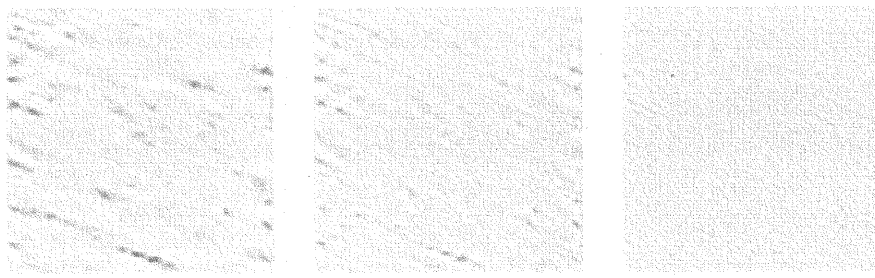

(a) CASE 1 (b) CASE 4 (c) CASE 10

Fig.18 Filtered STIs

yields patterns with clearer oblique traces. To examine the feature of surface wave celerity, the relation between the maximum wave length and the average celerity obtained from the filtered STI are shown in Fig.19(a). It should be noted that the average celerity decreases for the wave length less than four meters. This feature is qualitatively analogous to the small amplitude wave theory. Meanwhile, the celerity acquires almost the same value at about 4.5m/s for the range of larger wave length. Such a feature of constant celerity independent of the wave length cannot be explained by a simple gravity wave theory. Therefore, we can presume that the celerity obtained by STIV is not related to the gravity wave speed superposed on the flow. It is preferable to assume that the celerity exhibits water surface velocity and the inclined striped patterns are generated by water surface irregularity caused by the fluctuations of pressure and vertical velocity component inherent in open-channel turbulent flow. As evidence to support this assumption, it was found that a driftwood speed obtained for the same flood yields almost the same value as the velocity analyzed by STIV. This finding implies that the surface velocity can be measured by STIV only by paying attention to the relatively large scale surface pattern and small scale surface fluctuations are better to be filtered out for improving the measurement accuracy. Further examination is necessary to determine the most appropriate band pass range, but for the cases in Fig19, the case that covers the maximum wave length of about 3.5m, i.e. Case 4 seems to yield a more uniform orientation pattern than the other cases. On the other hand, the STI for Case 10 seems to contain a faint pattern with noise in the image and therefore is not suitable for flow measurement.

In order to verify the presumption presented above, the analyzed results of the STIs for different river floods are shown in Fig.19(b) and Fig.19(c). Both the Ichikawa River flood and the Uono River flood demonstrate similar characteristics to the results given in Fig.19. These figures all confirm the idea of using the surface ripple celerity as

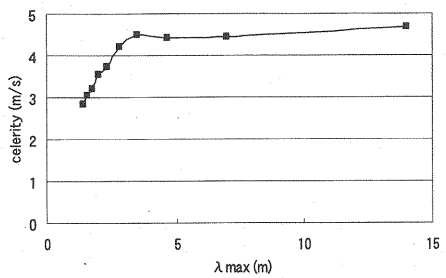

(a) Chikusa River

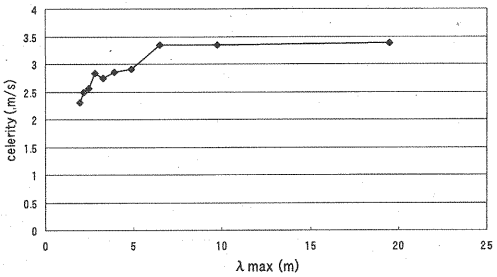

(b) Ichikawa River

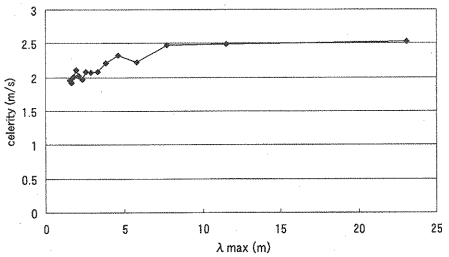

(c) Uono River

Fig.19 Relation between wavelength and celerity for other river floods

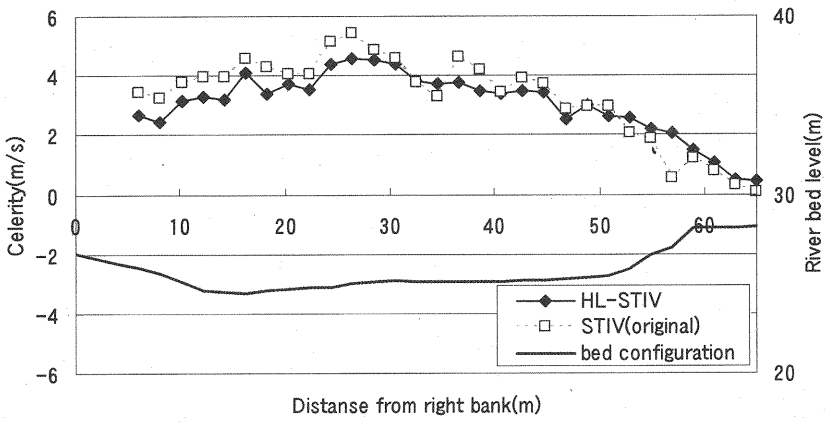

Fig.20 Transverse celerity distribution

representing the surface flow velocity.

MEASUREMENT OF DISCHARGE HYDROGRAPH

In order to examine the accuracy of discharge measurements by means of STIV, a transverse celerity distribution at each time is calculated using HL-STIV and the original STIV. An example at peak-level flow is shown in Fig.20 together with the cross-sectional bed elevation. The celerity gradually increases with the water depth in the center of the river and reaches the maximum speed of more than four meters per second. To compare the two versions of STIV, HL-STIV generates more stable variation than the original STIV. With the information concerning the water depth variation and the celerity distribution assumed here to be the same as the surface flow distribution, the flood discharge

at the section can be calculated and its hydrograph is shown in Fig.21. Generally, the two STIV techniques seem to generate similar results, but the original STIV failed to yield data at 14:10 on July 14 because of the too much adherence of raindrops to the lens filter. In order to compare the results with the other method, the discharge variation estimated from the rating curve at the section is also shown in Fig.21. The overall time variation of flood discharge by the rating curve agrees fairly well the image analysis methods especially with HL-STIV, except that the rating curve underestimates the peak discharge. The reason for this is that the difference is attributed to the lower accuracy of the float method that uses only a few floats for discharge measurement at this site and is incapable of measuring discharge at the section of the flood plain.

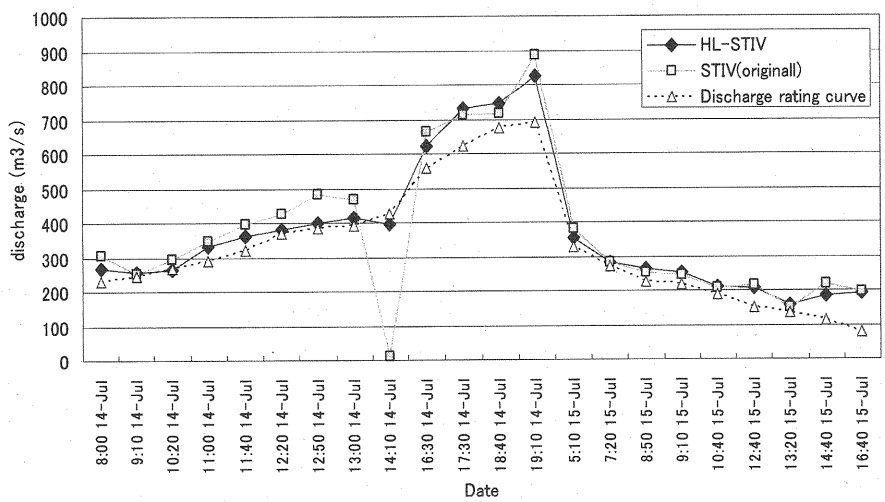

Fig.21 Comparison of discharge hydrograph by three methods

CONCLUSIONS

This research work proposes a series of new methods for measuring water surface velocity distribution from surface video images. The main idea of the method is to generate a space-time image (STI) for a line segment directed to the mean flow and measure the orientation angle of the oblique pattern appeared in the STI, from which the mean velocity averaged along the line segment can be obtained. This idea is useful because transverse special resolution is very high at one pixel in the image and the time averaged value can be directly measured from STI. Such features are quite different from the alternative image analysis method such as LSPIV which requires a large number of instantaneous data to obtain the mean value. In addition, it was shown that potential problems associated with night or rainy-day measurements can be overcome by applying a band pass filter to the transformed image by 2D-FFT, which all enhances the applicability of the proposed method. Moreover, the frequency analysis revealed that the short waves travel more slowly while longer waves are convected with constant speed and are comparable to the surface velocity. With such improvements whereby the STIV method introduced into the filtering process in frequency domain, the discharge hydrographs are obtained for the Chikusa River Flood in 2007 with a reasonable agreement with those estimated from the rating curve. This confirms the reliability of the proposed STIV technique. Further improvements of data acquisition and transfer system are necessary for establishing a real time flow measurement system.

REFERENCES

1. Dinehart, R. L. and Burau, J. R. : Averaged indicators of secondary flow in repeated acoustic Doppler current profiler crossings of bends, Water Resources Research, Vol.41, W09405(1-18), 2005.
2. Fujita, I. and Komura, S.: Application of video image analysis for measurements of river-surface flows, Annual Journal of Hydraulic Engineering, Japan Society of Civil Engineers, 38, pp.733-738 (in Japanese), 1994.
3. Fujita, I., Aya, S. and Deguchi, T. : Surface velocity measurement of river flow using video images of an oblique angle, Proceedings of the 27th Congress of IAHR, Theme B, Vol.1,San Francisco, CA, pp.227-232, 1997.
4. Fujita, I., Muste, M. and Kruger, A. : Large-scale particle image velocimetry for flow analysis in hydraulic engineering applications, Journal of Hydraulic Research, Vol.36, No.3, pp.397-414, 1998.
5. Fujita, I., Watanabe, H. and Tsubaki, R. : Development of a non-intrusive and efficient flow monitoring technique: The space time image velocimetry (STIV), International Journal of River Basin Management, 5(2), pp.105-114, 2007.
6. Hauet, A., Creutin, J.-D. and Belleudy, P.: Sensitivity study of large-scale particle image velocimetry measurement of river discharge using numerical simulations, Journal of Hydrology, 349(1-2), 178-190, doi:10.1016/j.jhydrol. 2007. 10.062., 2008.
7. Jodeau, M., Hauet, A., Paquier, A., Le Coz, A. and Dramais, G..: Application and evaluation of LS-PIV technique for the monitoring of river surface velocities in high flow conditions, Flow Measurement and Instrumentation, doi :10.1016/j.owmeasinst.2007.11.004, 2008.
8. Kantoush, S.A., De Cesare, G., Boillat, J.L. and Schleiss, A.J.: Flow field investigation in a rectangular shallow reservoir using UVP, LSPIV and numerical modelling, Flow measurement and Instrumentation, 19, pp.139-144, 2008.
9. Le Coz, Pierrefeu, J. G. and Paquier, A. : Evaluation of river discharges monitored by a fixed side-looking Doppler profiler, Water Resources Research, 44, W00D09, doi:10.1029/2008WR006967, 2008.
10. Meselhe, E.A., Peeva, T. and Muste, M.: Large scale image velocimetry for low velocity and shallow water flows, Journal of Hydraulic Engineering,130(9), pp.937-940, 2004.
11. Muste, M., Yu, K. and Spasojevic, M. : Practical aspects of ADCP data use for quantification of mean river flow characteristics; part I: Moving-vessel measurements, Flow Meas. Instrument., 15(1), pp.1?16, 2004.
12. Muste, M., Fujita, I., and Hauet, A.: Large-scale particle image velocimetry for measurements in riverine environments, Water Resources Research, 44, W00D19, doi:10.1029/2008WR006950, 2008.
13. Oberg, K. A. and Mueller, D. S. : Validation of streamflow measurements made with Acoustic Doppler Current Profilers, Journal of Hydraulic Engineering, 133(12), pp.1421?1432, 2007.
14. Teague, C. C., Barrick, D. E., Lilleboe, P. M. and Cheng, R. T.: River Sonde: measuring river surface velocity with UHF Radar, Book of Extended Abstracts, Hydraulic Measurements & Experimental Methods, pp.178-183, 2007.
15. Wang, C.J., Wen, B.Y., Ma, Z.G.., Yan, W.D. and Huang, X.J. : Measurement of River Surface Currents With UHF FMCW Radar Systems, J. of electromagnetic waves and applications, 21(3), pp. 375-386, 2007.

APPENDIX – NOTATION

The following symbols are used in this paper:

C = coherency of space-time image (STI);

$g(x,t)$ = grey level intensity on STI;
k = wave number;
x = horizontal coordinate along a line segment of STI;
t = vertical time coordinate of STI;
ϕ = orientation angle of image pattern; and
λ = wave length.

(Received Aug, 01, 2010 ; revised Jan, 28, 2011)